circCACNA1D drives pulmonary fibrosis by regulating pyruvate kinase M2 dimer-tetramer switching

YUJIE WANG[1,2*], XIAOTING LI[1*], MEIRONG WANG[3], NAILIANG ZHAI[2], MENGQI JIANG[1], BO LIU[2], CHANGJUN LV[2], SONGZI ZHANG[1,4], XIAODONG SONG[1,2] and JINJIN ZHANG[1,2]

[1]Department of Cellular and Genetic Medicine, Shandong Key Laboratory of Complex Medical Intelligence and Aging, Shandong Medical and Pharmaceutical University, Yantai, Shandong 264003, P.R. China; [2]Department of Respiratory and Critical Care Medicine, Shandong Medical and Pharmaceutical University Hospital, Shandong Medical and Pharmaceutical University, Binzhou, Shandong 256603, P.R. China; [3]Department of Medical Laboratory, Yantai Affiliated Hospital of Shandong Medical and Pharmaceutical University, Yantai, Shandong 264000, P.R. China; [4]The Medical Basic Research Innovation Center of Airway Disease in North China, Ministry of Education of China, College of Basic Medical Sciences, Jilin University, Changchun, Jilin 130021, P.R. China

Received March 4, 2026; Accepted June 25, 2026

DOI: 10.3892/ijmm.2026.5931

Abstract. Pulmonary fibrosis is a progressive and fatal interstitial lung disease characterized by aberrant fibroblast activation and excessive extracellular matrix deposition. Circular RNAs (circRNAs) have emerged as critical regulators of fibrotic pathogenesis. However, their mechanistic roles remain incompletely defined. In the present study, circCACNA1D was identified as a novel driver of pulmonary fibrosis progression through direct interaction with pyruvate kinase M2 (PKM2). Specifically, circCACNA1D binds PKM2 and promotes its nuclear translocation and dimerization. This process is facilitated by desuccinylation at conserved lysine residues (K135, K166 and K270). The conformational shift from the tetrameric to the dimeric state reprograms cellular metabolism toward aerobic glycolysis and activates a pro-fibrotic transcriptional program, including direct upregulation of KIF4A. In addition, the pharmacological stabilization of PKM2 tetramers with TEPP-46 attenuated fibrotic phenotypes *in vitro* and alleviated bleomycin-induced pulmonary fibrosis in mice. These findings define a previously unrecognized circRNA-driven axis that coordinates PKM2 conformational switching, metabolic reprogramming and transcriptional activation, and suggest a potential therapeutic strategy for pulmonary fibrosis.

Correspondence to: Dr Jinjin Zhang or Dr Xiaodong Song, Department of Cellular and Genetic Medicine, Shandong Key Laboratory of Complex Medical Intelligence and Aging, Shandong Medical and Pharmaceutical University, 318 Gangcheng East Street, Laishan, Yantai, Shandong 264003, P.R. China
E-mail: jjinzhang@bzmc.edu
E-mail: songxd71@bzmc.edu.cn

*Contributed equally

Key words: circCACNA1D, pyruvate kinase M2, dimer-tetramer switch, succinylation, pulmonary fibrosis, metabolic reprogramming, kinesin family member 4A

Introduction

Idiopathic pulmonary fibrosis is a progressive and fatal interstitial lung disease characterized by aberrant fibroblast activation and excessive extracellular matrix deposition, leading to irreversible scarring and respiratory failure (1,2). Although the understanding of its pathogenesis has advanced, the molecular mechanisms underlying fibroblast metabolic reprogramming, a hallmark of fibrosis progression, remain incompletely defined (3,4). Current therapeutic agents, including pirfenidone and nintedanib, primarily attenuate disease progression rather than reverse established fibrosis. Therefore, identifying novel pathogenic drivers and therapeutic targets remains essential (5,6).

A growing body of evidence suggests that metabolic reprogramming is a hallmark of fibrotic remodeling (4,7,8). Similar to rapidly proliferating cells, activated fibroblasts upregulate aerobic glycolysis to support biosynthesis, redox balance, contractility and extracellular matrix production (9,10). In pulmonary fibrosis, this shift is not merely a secondary consequence of injury, but a critical driver of myofibroblast persistence and tissue remodeling. These observations have sparked interest in metabolic enzymes as potential upstream regulators of fibrogenesis.

Among these enzymes, pyruvate kinase M2 (PKM2) has emerged as a particularly critical metabolic and signaling node (11-13). PKM2, an alternatively spliced isoform of the PKM gene, exists in a dynamic equilibrium between a highly active tetrameric form and a less active dimeric form (14). Tetrameric PKM2 efficiently catalyzes the final step of glycolysis in the cytosol, whereas dimeric PKM2 favors the diversion of glycolytic intermediates into anabolic pathways and can translocate to the nucleus, where it functions as a protein kinase or transcriptional co-activator (9,11,15). Recent studies support a direct role for PKM2 in organ

fibrosis. For example, in pulmonary fibrosis, PKM2 has been shown to promote disease progression by stabilizing TGF-β receptor I and amplifying profibrotic signaling (16). In addition, in the kidneys, PKM2-dependent glycolytic remodeling has been shown to drive pericyte activation and fibrogenic transition (17), whereas the pharmacological activation of PKM2 with TEPP-46 suppresses aberrant glycolysis and renal fibrosis (18). Furthermore, in the liver, enforced PKM2 tetramerization restrains hepatic stellate cell activation and protects against fibrosis (19). Finally, studies using liver and vascular injury models further support PKM2 as a determinant of profibrotic metabolic remodeling (20,21). Taken together, these findings indicate that the dimer-tetramer equilibrium of PKM2 is functionally critical in fibrosis.

Diverse post-translational modifications (PTMs) regulate PKM2 activity, localization and oligomeric state. Among these, lysine succinylation has attracted increasing interest owing to its ability to notably alter residue charge and reshape protein conformation (22). Previoius studies have indicated that succinylation-dependent PKM2 dimerization contributes to fibrosis-related phenotypes in the heart and other pathological contexts (23,24). SIRT5 is the most well-characterized desuccinylase and regulates multiple metabolic enzymes, including PKM2 (25-27). However, the upstream mechanisms that control PKM2 succinylation-dependent conformational switching in pulmonary fibrosis remain largely unknown. In particular, whether a disease-associated non-coding RNA directly modulates PKM2 succinylation and thereby influences its dimer-tetramer equilibrium remains elusive.

Circular RNAs (circRNAs) are covalently closed RNA molecules generated by back-splicing of precursor transcripts (28-30). As they lack free 5' and 3' ends, circRNAs often exhibit enhanced resistance to exonucleases, although their stability in biological and clinical specimens is context-dependent (31,32). circRNAs have emerged as key regulators of fibrotic disorders, such as pulmonary fibrosis, in which they modulate fibroblast activation, extracellular matrix production, inflammatory signaling and metabolic adaptation (1,3,33,34). The majority of mechanistic studies have focused on their roles as microRNA sponges or modulators of RNA-binding proteins (35). However, more recently, circRNAs have also been recognized as direct protein-binding molecules capable of altering protein localization, enzymatic activity and assembly into functional complexes (35,36). This emerging concept raises a critical, yet unexplored possibility, whereby specific circRNAs may directly regulate PKM2 conformational dynamics and metabolic signaling in pulmonary fibrosis.

In the present study, circCACNA1D was identified as an upregulated circRNA in fibrotic lungs and activated fibroblasts. In addition, it was demonstrated that circCACNA1D directly binds to PKM2, promotes desuccinylation at K135, K166 and K270, and shifts PKM2 from the tetrameric toward the dimeric state. This conformational switch enhances glycolytic reprogramming and nuclear PKM2 signaling, leading to the induction of the downstream effector kinesin family member 4A (KIF4A) and the promotion of fibroblast activation and pulmonary fibrosis. These findings define a circCACNA1D-PKM2 axis that links circRNA-mediated protein regulation to metabolic plasticity in pulmonary fibrosis.

Materials and methods

Cells, cell culture and treatments. The human fetal lung fibroblast cell line, MRC-5, was obtained from The American Type Culture Collection. Cells were cultured in minimum essential medium (Gibco; Thermo Fisher Scientific, Inc.) supplemented with 10% fetal bovine serum (Gibco; Thermo Fisher Scientific, Inc.), 1% penicillin-streptomycin solution (cat. no. CM0004-100ML; Shandong Sparkjade Scientific Instruments Co., Ltd.), 1% sodium pyruvate (cat. no. 11360070; Gibco; Thermo Fisher Scientific, Inc.), 1% GlutaMAX (cat. no. 35050061; Gibco; Thermo Fisher Scientific, Inc.) and 1% non-essential amino acids (cat. no. 11140050; Gibco; Thermo Fisher Scientific, Inc.). The cells were maintained at 37˚C in a humidified atmosphere containing 5% CO_2.

MRC-5 cells were cultured as aforementioned. To establish an *in vitro* model of fibrosis, the cells were exposed to 5 ng/ml recombinant human TGF-β1 (cat. no. PHG9202; Gibco; Thermo Fisher Scientific, Inc.) for 0, 48 or 72 h. For gain- and loss-of-function experiments, the cells were transfected with a circCACNA1D overexpression (OE) plasmid, small interfering RNAs (siRNAs) targeting circCACNA1D (sense, CAA AUCAUA ACUUGAGGCATT; antisense, UGCCUCAAG UUAUGAUUUGTT) and KIF4A (sense, CGUCAAGCGCAG AUGUCUATT; antisense, UAGACAUCUGCGCUUGAC GTT), a PKM2-NLS (nuclear localization signal) plasmid, a KIF4A OE plasmid or corresponding negative controls (si-NC sense, UUCUCCGAACGUGUCACGUTT; antisense, ACG UGACACGUUCGGAGAATT) (Keyybio) using Lipo3.0 (cat. no. BMU111-CN; Abbkine Scientific Co., Ltd.) according to the manufacturer's instructions. For siRNA transfection, the final concentration of each siRNA was 50 nM. The siRNA-Lipo3.0 complexes were incubated at room temperature for 15 min before being added to the cells. Following 6 h of transfection, the medium was replaced with fresh complete medium, and cells were harvested 48 h post-transfection for subsequent analyses. The transfection efficiency was verified at 48 h post-transfection, whereby circCACNA1D OE and siRNA knockdown were confirmed using reverse transcription-quantitative PCR (RT-qPCR), with only experiments achieving >5-fold OE or >70% reduction relative to the controls included in downstream analyses (Fig. S1A and B). In addition, the expression levels of PKM2-NLS and KIF4A were confirmed using western blot analysis (Fig. S1C-E). In co-transfection rescue experiments, MRC-5 cells were first transfected with si-circCACNA1D/si-KIF4A (50 nM) or a scrambled siRNA control. A total of 6 h following the initial transfection, the cells were transfected with the PKM2-NLS plasmid (2 μg/well; 6-well plate format) or an empty vector control, followed by TGF-β1 (5 ng/ml) stimulation for 48 h. In all co-transfection experiments, total nucleic acid was kept consistent across groups using empty vectors or scrambled siRNAs (negative controls) as appropriate. For pharmacological intervention, TGF-β1-stimulated cells were treated with TEPP-46 (MedChemExpress; cat. no. HY-18657) at the indicated concentrations for 48 h.

Animal model of pulmonary fibrosis. All animal procedures were approved by The Animal Ethics Committee of Shandong Medical and Pharmaceutical University, Yantai,

China (approval no. 2021-355). Male C57BL/6 mice (age, 6 weeks; weighing 20-24 g) were purchased from The Nanjing University Model Animal Research Center. A total of 24 mice were used in the present study. All mice were housed under specific pathogen-free barrier conditions on a 12-h light/dark cycle (lights on from 07:00 to 19:00) at 22±2˚C with 50±10% relative humidity. Light intensity within the cage position was maintained at 15-20 lux to stabilize circadian rhythms. As mice are nocturnal rodents, all sample collection and experimental procedures were fixed to the same time window during the light phase to avoid potential interference from circadian variation. Mice were randomly assigned to the following four groups (n=6/group): i) Sham control (saline); ii) bleomycin (BLM); iii) BLM + vehicle (DMSO); and iv) BLM + TEPP-46.

Pulmonary fibrosis was induced by a single intratracheal instillation of BLM (5 mg/kg body weight in 50 μl sterile saline/mouse; Nippon Kayaku Co., Ltd.) using a Penn-Century MicroSprayer (Penn-Century Inc.). The mice in the sham group received an equal volume of sterile saline. From day 3 following instillation, mice in the TEPP-46 group received daily oral gavage of TEPP-46 (cat. no. HY-18657; MedChemExpress) (30 mg/kg in the vehicle), whereas the vehicle group received an equal volume of 2.5% DMSO in saline. On day 28, lung tissues were harvested for molecular and histopathological analyses.

Animal euthanasia. In accordance with the American Veterinary Medical Association Guidelines for the Euthanasia of Animals (2020 Edition), all animals were humanely euthanized at the end of the experimental protocol. At the experimental endpoint (day 28 after BLM instillation), all mice were deeply anesthetized by intraperitoneal injection with pentobarbital sodium (150 mg/kg body weight). Following the loss of pedal reflex, euthanasia was performed by cervical dislocation. After which, lung tissues were immediately harvested for subsequent analyses.

RNA immunoprecipitation (RIP)-PCR analysis. RIP assays were performed using an RNA immunoprecipitation kit (cat. no. P0101, Guangzhou Geneseed Biotech. Co., Ltd.) according to the manufacturer's instructions. MRC-5 cells (~1x10^7 cells/sample) were lysed in lysis buffer supplemented with 1% (v/v) protease inhibitor and 1% (v/v) RNase inhibitor (included with the immunoprecipitation kit). Lysates were incubated overnight at 4˚C with magnetic beads pre-conjugated to 5 μg anti-PKM2 antibody (cat. no. 4053S; Cell Signaling Technology, Inc.) or normal rabbit IgG (cat. no. 2729S; Cell Signaling Technology, Inc.) as a negative control. Following extensive washing (with washing buffer provided with the kit), RNA was extracted using the RNA extraction reagent provided with the RNA immunoprecipitation kit (Guangzhou Geneseed Biotech. Co., Ltd.) according to the manufacturer's instructions, and reverse-transcribed using the Evo M-MLV reverse transcription kit (AG11706, Hunan Accurate Bio-Medical Technology Co., Ltd.). The enrichment of circCACNA1D was quantified using RT-qPCR with SYBR-Green (SYBR-Green Premix Pro Taq HS; Hunan Accurate Bio-Medical Technology Co., Ltd.). The qPCR program consisted of an initial denaturation at 94˚C for 600 sec, followed by 45 cycles of 94˚C for 5 sec, 60˚C for 32 sec and 72˚C for 30 sec. The following primer sequences were used: circCACNA1D forward, 5'-GCC AATTGTGTGGCCTTAGCT-3' and reverse, 5'-CCTCTT GCATAGTTTGCCTCAAG-3'. Normal IgG was used as a negative control, and relative enrichment was calculated using the $2^{-\Delta\Delta Cq}$ method (37).

RNA pull-down and mass spectrometry. Biotin-labeled RNA probes complementary to the sense sequence of circCACNA1D and an antisense control were synthesized by Guangzhou RiboBio Co., Ltd. Probes were conjugated to streptavidin magnetic beads (cat. no. Bes5102; BersinBio), and whole-cell lysates from MRC-5 cells were incubated with the probe-bound beads overnight at 4˚C. Following stringent washing with the washing buffer provided with the kit, the magnetic beads were collected using a magnetic stand at room temperature. Bound proteins were then eluted by boiling at 98˚C for 10 min and separated by 10% SDS-PAGE. Gels were silver-stained, and the specific band at ~60 kDa was excised for in-gel tryptic digestion. Peptides were analyzed by liquid chromatography-tandem mass spectrometry (LC-MS/MS) using an Orbitrap Exploris 480 mass spectrometer (Thermo Fisher Scientific, Inc.). For LC-MS/MS identification of succinylation sites, raw data were analyzed using MaxQuant (v1.6.15.0). Searches were performed against the *Mus musculus* reference proteome (Mus_musculus_10090_SP_20220107.fasta; 17,097 sequences). The false discovery rate was set to <1% at the peptide and protein levels, and each identified protein was required to contain at least one unique peptide. The mass spectrometry proteomics data have been submitted to the ProteomeXchange Consortium through the PRIDE partner repository with the dataset identifier PXD075455, and are accessible at https://www.ebi.ac.uk/pride/archive/projects/PXD075455.

RT-qPCR. Total RNA was extracted from cells or tissues using TRIzol reagent (AG21102; Hunan Accurate Bio-Medical Technology Co., Ltd.), and cDNA was synthesized using the Evo M-MLV RT Premix Kit (AG11706, Hunan Accurate Bio-Medical Technology Co., Ltd). RT-qPCR was performed on a Rotor-Gene 3000 real-time PCR system using SYBR-Green Premix Pro Taq HS (Hunan Accurate Bio-Medical Technology Co., Ltd). β-actin was used as an internal control, and relative expression levels were calculated using the $2^{-\Delta\Delta Cq}$ method (37). The primer sequences are provided in Table SI. Melting curve analysis was performed after each qPCR run to confirm the specificity of amplification, and all primer pairs produced a single melting peak. Primer amplification efficiencies, validated by standard curve analysis using serial dilutions of cDNA, ranged from 90 to 110%. The stability of β-actin as a reference gene was confirmed under all experimental conditions, with no significant variation in Ct values observed between treatment groups.

Immunofluorescence and RNA fluorescence in situ hybridization (FISH). MRC-5 cells grown on coverslips were fixed with 4% paraformaldehyde and permeabilized with 0.5% Triton X-100. A Cy3-labeled probe (30 nucleotides in length) targeting the circCACNA1D back-splice junction (Guangzhou RiboBio Co., Ltd.) was used for FISH. Hybridization was performed overnight at 37˚C in a humidified chamber

according to the manufacturer's instructions. Following FISH, the cells were blocked with 10% goat serum (cat. no. C0265; Beyotime Biotechnology) at room temperature for 1 h and incubated overnight at 4˚C with anti-PKM2 antibody (1:50; cat. no. 4053S; Cell Signaling Technology, Inc.). After washing with PBS, the cells were incubated with Alexa Fluor 488-conjugated secondary antibody (1:200; cat. no. S0018; Affinity Biosciences) for 30 min at room temperature in the dark. Nuclei were counterstained with DAPI (Beijing Solarbio Science & Technology Co., Ltd.) at room temperature for 8 min, and images were captured using a laser-scanning confocal microscope (Stellaris 5; Leica Microsystems GmbH).

Nuclear-cytoplasmic fractionation and western blot analysis. Nuclear and cytoplasmic fractions were isolated using NE-PER™ Nuclear and Cytoplasmic Extraction Reagents (Thermo Fisher Scientific, Inc.) according to the manufacturer's protocol. For total protein extraction, cells or tissues were lysed in RIPA buffer supplemented with protease and phosphatase inhibitors. Protein concentrations were measured using a BCA assay. Equal amounts of protein (20 μg/lane) were separated by 10% SDS-PAGE and transferred to PVDF membranes by wet transfer at 200 mA for 120 min on ice. The membranes were blocked with 5% non-fat milk and incubated overnight at 4˚C with primary antibodies. Following incubation with HRP-conjugated secondary antibodies (1:2,000; SAB48169; Bioswamp, Wuhan Bienle Biotechnology Co., Ltd.) at room temperature for 1 h, protein bands were detected using an enhanced chemiluminescence kit (ED0015-B; Shandong Sparkjade Scientific Instruments Co., Ltd.). Densitometric quantification was performed using ImageJ software (National Institutes of Health). The relative expression level of each target protein was calculated as the ratio of target band intensity to that of β-tubulin on the same membrane and was further normalized to the control group (set as 1). Results are expressed as the fold change relative to the control. Primary antibodies included: PKM2 (1:1,000; cat. no. 4053S; Cell Signaling Technology, Inc.), α-SMA (1:1,000; cat. no. AF1032; Affinity Biosciences), Vimentin (1:1,000; cat. no. MAB61559; Bioswamp; Wuhan Bienle Biotechnology Co., Ltd.), collagen I (1:1,000; cat. no. AF7001; Affinity Biosciences), β-actin (1:5,000; cat. no. AF7018; Affinity Biosciences), β-tubulin (1:5,000; cat. no. AF7011; Affinity Biosciences) and Lamin B1 (1:5,000; cat. no. RMAB60267; Bioswamp; Wuhan Bienle Biotechnology Co., Ltd.).

Analysis of the PKM2 oligomeric state (dimer/tetramer). The oligomeric state of PKM2 was assessed by chemical cross-linking followed by 6% non-reducing SDS-PAGE. Cell lysates were incubated with freshly prepared disuccinimidyl suberate (Thermo Fisher Scientific, Inc.) dissolved in anhydrous DMSO at a final concentration of 2 mM for 30 min at room temperature. The reaction was quenched with 1 M Tris-HCl (pH 7.5) to a final concentration of 20 mM. Samples were separated on a 6% non-reducing polyacrylamide gel at 80 V for 2 h, and then transferred to PVDF membranes by wet transfer at 200 mA for 2.5 h on ice. Western blot analysis was performed under non-reducing conditions, without β-mercaptoethanol in the loading buffer, using an anti-PKM2 antibody (1:1,000; cat. no. 4053S; Cell Signaling Technology, Inc.). The remaining steps were the same as the western blot protocol described above.

Co-immunoprecipitation (Co-IP) and succinylation modification analysis. For Co-IP assays, cell lysates were prepared using IP lysis buffer [provided with the Immunoprecipitation (IP/CoIP) kit; abs955-50T; Absin Bioscience Inc.]. To assess PKM2 succinylation, 500 μg of total protein lysates were incubated overnight at 4˚C with anti-PKM2 antibody (1:1,000; cat. no. 4053S; Cell Signaling Technology, Inc.). Immune complexes were captured using Protein A/G agarose beads (abs955-50T; Absin Bioscience Inc.). Following extensive washing, with 1x washing buffer (provided in the same kit), bound proteins were eluted by boiling at 98˚C for 10 min and subjected to western blot analysis, which was performed as described above, using a pan-anti-succinyllysine antibody (1:500, PTM BIO, #PTM-401). Centrifugation steps were performed at 13,523 g for 1 min at room temperature.

Wound healing and cell proliferation assays. For wound healing assays, the MRC-5 cells were seeded in 96-well plates and grown to 90% confluency. A uniform scratch was generated using the IncuCyte S3 scratcher. Cells were washed and cultured in serum-free medium with or without the indicated treatments. Wound closure was monitored every 3 h using the IncuCyte S3 Live-Cell Analysis System (Sartorius, Germany) with a 10X objective. Wound healing was quantified by wound density, which was automatically calculated using IncuCyte S3 software. Cell proliferation was assessed by measuring confluence over time at 4-h intervals in 96-well plates using the same system.

Measurement of pyruvate kinase activity and lactate production. Pyruvate kinase activity was measured using a Pyruvate Kinase Activity Assay kit (cat. no. BC2205; Beijing Solarbio Science & Technology Co., Ltd.) according to the manufacturer's instructions. Lactate concentrations in cell culture supernatants were determined using a Lactate Assay kit (cat. no. BC2235; Beijing Solarbio Science & Technology Co., Ltd.).

Histopathological staining (H&E and Masson's trichrome staining). Lung tissues were fixed in 4% paraformaldehyde at room temperature for 1 h, dehydrated through a graded ethanol series and embedded in paraffin. Serial sections (4-μm thick) were prepared using a Leica RM2255 rotary microtome. For morphological evaluation, sections were stained with H&E using a commercial kit (cat. no. G1120; Beijing Solarbio Science & Technology Co., Ltd.) at room temperature, with hematoxylin staining for 5-10 min and eosin staining for 5 min. Collagen deposition was assessed by Masson's trichrome staining according to the manufacturer's protocol (Beijing Solarbio Science & Technology Co., Ltd.) at room temperature, with Ponceau S staining for 5-10 min and aniline blue staining for 1-2 min. Following staining, the sections were dehydrated in absolute ethanol, cleared in xylene and mounted with neutral resin. Images were captured using an Olympus light microscope (Olympus Corporation).

Lung function measurements. Pulmonary function was evaluated using the AniRes2005 Animal Lung Function Analysis

System (Bestlab Technology Co., Ltd.). Mice were anesthetized by intraperitoneal injection of 2.5% Avertin (250 mg/kg). Following deep anesthesia, a midline cervical incision was made to expose the trachea, which was intubated and secured with a suture. Mice were placed in a whole-body plethysmography chamber, which was preset with an initial negative pressure of 30 cmH_2O, a respiratory rate of 65 breaths/min and an inspiration-to-expiration ratio of 20:10. The automated mode was initiated to record forced vital capacity (FVC) and lung compliance during passive inhalation to the target pressure followed by passive exhalation.

RNA sequencing and bioinformatics analysis. Total RNA was extracted from the MRC-5 cells under four conditions: i) Control; ii) TGF-β1; iii) TGF-β1 + vehicle (DMSO); and iv) TGF-β1 + TEPP-46. RNA quality was evaluated prior to library preparation. Libraries were constructed and sequenced on an Illumina NovaSeq 6000 platform by Shenzhen E-Gene Biotechnology Co., Ltd. Raw reads were processed, aligned to the reference genome and quantified, with differential gene expression analysis performed using DESeq2. Gene Ontology (GO) and Kyoto Encyclopedia of Genes and Genomes (KEGG) pathway enrichment analyses were conducted using clusterProfiler. Venn diagrams were generated to identify overlapping differentially expressed genes. The raw sequencing data generated in this study are openly available in the NCBI SRA database accessible with the following link: https://www.ncbi.nlm.nih.gov/sra/PRJNA1475466.

Chromatin immunoprecipitation quantitative PCR (ChIP-qPCR). ChIP assays were conducted using the Simple ChIP Enzymatic Chromatin IP kit (cat. no. 9002; Cell Signaling Technology, Inc.). MRC-5 cells were cross-linked with 1% formaldehyde (cat. no. F809702; Shanghai Macklin Biochemical Co., Ltd.) at room temperature for 10 min. Crosslinking was terminated by the addition of 2.5 M glycine (cat. no. MB4166; MeilunBio) for 5 min. Chromatin was fragmented to 200-500 bp by sonication and immunoprecipitated overnight at 4˚C with anti-PKM2 antibody (5 μl per IP reaction; cat. no. 15822-1-AP; Proteintech Group, Inc.) or normal rabbit IgG (cat. no. 2729P; Cell Signaling Technology, Inc.). The enrichment of specific genomic regions, including the KIF4A promoter, was quantified by qPCR. Primers targeting predicted PKM2-binding sites are listed in Table SI. Due to the head-to-head genomic arrangement of KIF4A and PDZD11, the ChIP-qPCR primers targeting the KIF4A promoter region also amplify the overlapping PDZD11 promoter. Nevertheless, subsequent expression analyses confirmed that PDZD11 is not regulated under the experimental conditions used in this study.

Statistical analysis. For *in vitro* experiments, assays were performed in triplicate as independent biological replicates. For *in vivo* experiments, each group contained 6 mice, and representative data are shown. Statistical analyses were performed using GraphPad Prism 8.0.2 (263) software (Dotmatics). Student's t-test (unpaired t-test) was used for comparisons between two groups, and one-way ANOVA followed by Tukey's test was applied for comparisons among multiple groups. Data are presented as the mean ± SD. $P<0.05$ was considered to indicate a statistically significant difference.

Results

Identification of PKM2 as a direct binding partner of circCACNA1D in pulmonary fibrosis. To establish an *in vitro* model of pulmonary fibrosis, MRC-5 cells were exposed to TGF-β1 for 48 and 72 h, as previously described (38,39). Scratch-wound healing assays revealed a time-dependent increase in cell migration (Fig. 1A and B), and cell proliferation also increased over time (Fig. 1C). Western blot analysis demonstrated the significant upregulation of fibrotic markers, including α-SMA, vimentin and collagen I, following TGF-β1 stimulation. Densitometric quantification from three independent experiments confirmed these changes (Fig. 1D and E). Immunofluorescence staining further revealed progressively enhanced α-SMA signals, indicating the acquisition of a myofibroblast phenotype (Fig. 1F).

It was previously reported that circ0066187, now termed circCACNA1D, is upregulated in pulmonary fibrosis and exerts pro-fibrotic effects partly by sponging miR-29b-2-5p (33). Therefore, the present study examined whether circCACNA1D also functions through direct RNA-protein interactions. As circCACNA1D is predominantly cytoplasmic and has documented fibrogenic activity, it was hypothesized that it may function as a protein scaffold or decoy to regulate key fibrotic mediators. An unbiased RNA pull-down assay followed by LC-MS/MS was performed using a biotin-labeled sense probe targeting circCACNA1D. A specific protein band at ~60 kDa was enriched by the sense probe, but not by the antisense control (Fig. 1G). Mass spectrometry identified PKM as a candidate binding protein (Fig. 1H). Given the molecular weight and functional relevance, the present study focused on PKM2.

The interaction was validated using complementary biochemical approaches. RNA pull-down followed by western blot analysis confirmed the specific enrichment of PKM2 by the circCACNA1D sense probe (Fig. 1I). RIP assays further revealed that TGF-β1 stimulation significantly increased circCACNA1D enrichment by the anti-PKM2 antibody compared with the IgG control (Fig. 1J). Combined RNA-FISH and immunofluorescence analysis demonstrated increased circCACNA1D expression and the enhanced nuclear accumulation of PKM2 following exposure of the cells to TGF-β1, with marked co-localization signals (Fig. 1K). These findings indicate that circCACNA1D directly interacts with PKM2 during pulmonary fibrosis.

circCACNA1D promotes PKM2 nuclear translocation and dimerization. Given the TGF-β1-induced nuclear accumulation of PKM2, whether circCACNA1D regulates this process was then assessed. Nuclear-cytoplasmic fractionation followed by western blot analysis revealed that TGF-β1 stimulation or circCACNA1D OE (OE circRNA) significantly increased nuclear PKM2 levels. By contrast, circCACNA1D knockdown (si-circRNA) markedly reduced TGF-β1-induced PKM2 nuclear translocation (Fig. 2A). Immunofluorescence analysis confirmed these findings. Specifically, nuclear PKM2 signals were enhanced following TGF-β1 treatment or circCACNA1D OE, whereas circCACNA1D silencing resulted in predominant cytoplasmic localization (Fig. 2B).

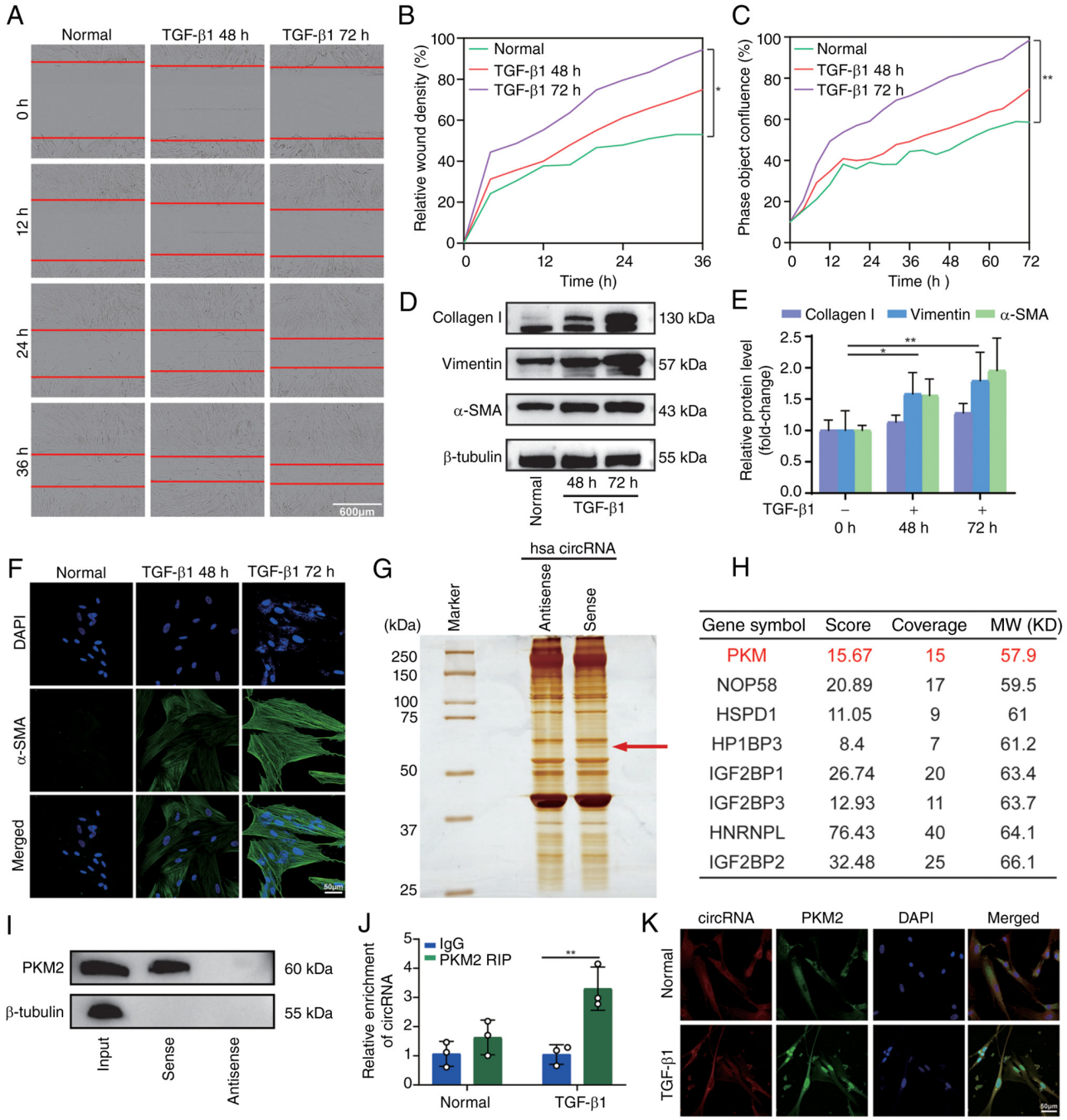

Figure 1. Identification of PKM2 as a direct binding partner of circCACNA1D in pulmonary fibrosis. (A) Scratch-wound healing assay of MRC-5 fibroblasts treated with TGF-β1 (5 ng/ml) for 0, 48 and 72 h. (B) Quantitative analysis of wound closure. (C) Proliferation of MRC-5 cells treated with TGF-β1 for the indicated times was monitored using the IncuCyte S3 live-cell analysis system. (D) Western blot analysis of fibrotic markers (α-SMA, vimentin and collagen I) in MRC-5 cells stimulated with TGF-β1 for 48 and 72 h. β-tubulin served as the loading control. (E) Quantitative analysis of the results of western blot analysis. (F) Representative immunofluorescence images demonstrating α-SMA (green) expression in MRC-5 cells following exposure to TGF-β1 for 0, 48 and 72 h. Nuclei were stained with DAPI (blue). (G) Silver staining of proteins pulled down by biotinylated circCACNA1D sense or antisense control probes. (H) Arrow indicates the specific ~60 kDa band identified by mass spectrometry. (I) Western blot validation of PKM2 enrichment in the RNA pull-down assay using a circCACNA1D sense probe. Input lysate served as the positive control. (J) RIP-qPCR analysis illustrating the enrichment of circCACNA1D by anti-PKM2 antibody in MRC-5 cells with or without TGF-β1 (5 ng/ml; 48 h). Normal IgG served as a negative control. (K) RNA-FISH detection of circCACNA1D (red) combined with immunofluorescence staining of PKM2 (green) in MRC-5 cells treated with or without TGF-β1. Nuclei were stained with DAPI (blue; scale bar, 50 μm). *P<0.05, **P<0.01. PKM2, pyruvate kinase M2; circRNA, circular RNA; RIP, RNA immunoprecipitation; FISH, fluorescence *in situ* hybridization.

PKM2 performs distinct functions depending on its oligomeric state, acting as a high-activity tetramer in the cytoplasm and as a low-activity dimer with transcriptional co-activator activity in the nucleus. It was first determined whether TGF-β1 alters endogenous PKM2 conformation. Chemical cross-linking followed by non-reducing SDS-PAGE revealed that TGF-β1 induced a shift from tetrameric PKM2 (~240 kDa) to the dimeric form (~120 kDa; Fig. 2C). Subsequently, the present study examined whether circCACNA1D influences this conformational balance. CircCACNA1D OE increased the proportion of dimeric PKM2 and reduced tetrameric PKM2, as determined by cross-linking and non-reducing SDS-PAGE

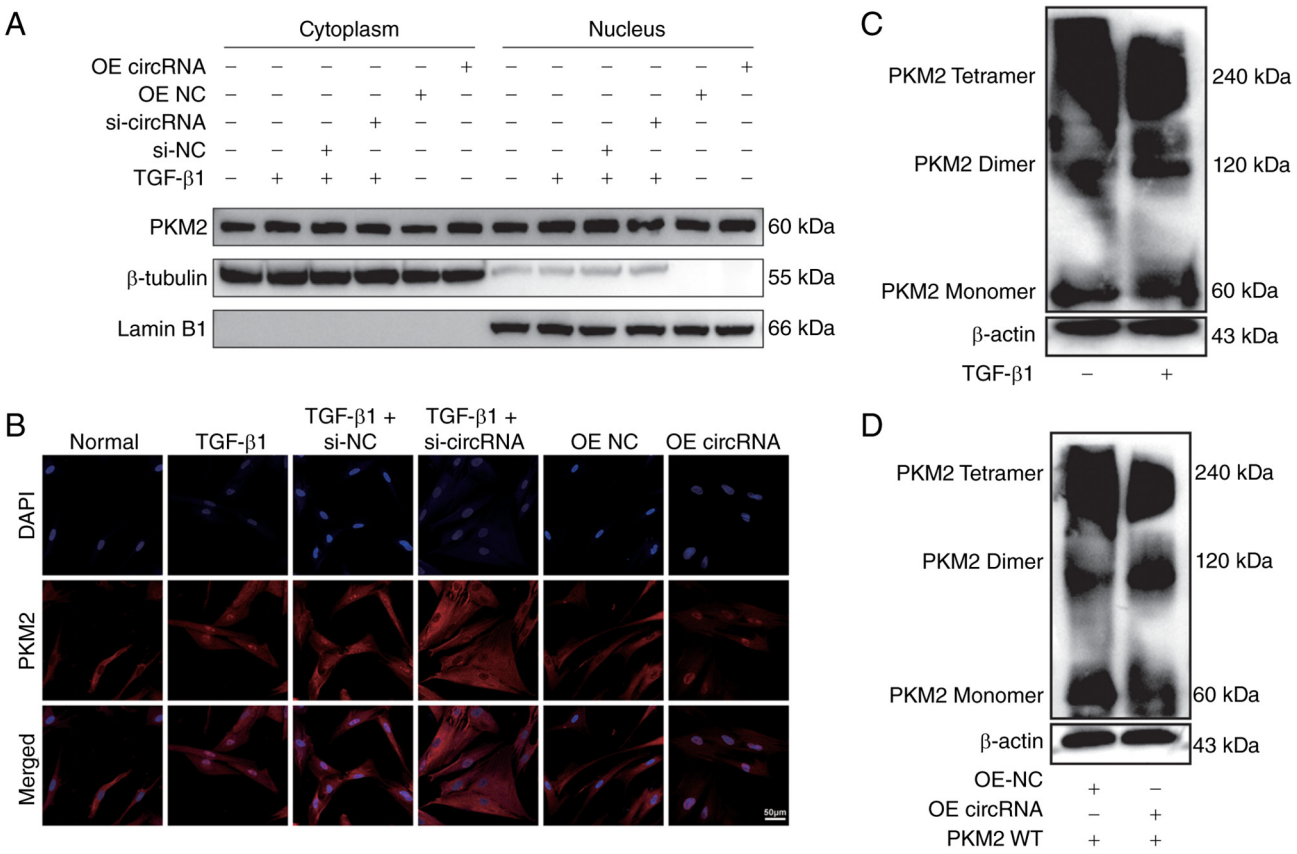

Figure 2. circCACNA1D promotes PKM2 nuclear translocation and dimerization. (A) Nuclear-cytoplasmic fractionation and western blot analysis of PKM2 in MRC-5 cells treated with TGF-β1 (5 ng/ml; 48 h), transfected with circCACNA1D overexpression plasmid (OE circRNA), or transfected with circCACNA1D knockdown (si-circRNA). Lamin B1 and β-tubulin served as nuclear and cytoplasmic markers, respectively. (B) Immunofluorescence staining of PKM2 (red) in MRC-5 cells under the indicated treatments. Nuclei were stained with DAPI (blue; scale bar, 50 μm). (C) Chemical cross-linking followed by non-reducing SDS-PAGE and western blot analysis to assess PKM2 oligomerization in MRC-5 cells treated with or without TGF-β1. (D) Chemical cross-linking followed by non-reducing SDS-PAGE and western blot analysis to assess PKM2 oligomerization in MRC-5 cells transfected with circCACNA1D or an empty vector. Positions of tetrameric (~240 kDa) and dimeric (~120 kDa) PKM2 are indicated. PKM2, pyruvate kinase M2; circRNA, circular RNA; NC, negative control; WT, wild-type.

(Fig. 2D). These results indicate that circCACNA1D promotes both nuclear translocation and dimerization of PKM2, similar to the effect of TGF-β1.

circCACNA1D promotes PKM2 desuccinylation at specific lysine residues to facilitate dimer formation. To define the molecular mechanism underlying circCACNA1D-mediated PKM2 dimerization, PTMs were examined, with a focus on lysine succinylation. Immunoprecipitation of PKM2 followed by western blot analysis with a pan-anti-succinyllysine antibody revealed that TGF-β1 significantly reduced PKM2 succinylation in MRC-5 cells (Fig. 3A). circCACNA1D OE further decreased PKM2 succinylation levels (Fig. 3B), suggesting that circCACNA1D promotes PKM2 desuccinylation under fibrotic conditions.

To identify specific residues, PKM2 was immunoprecipitated from lung tissues of BLM-treated and control mice and analyzed by LC-MS/MS. A total of three lysine residues, K135, K166 and K270, exhibited significantly reduced succinylation in fibrotic tissues. Representative MS/MS spectra confirmed succinyllysine modification at these sites (Fig. 3C). Sequence alignment demonstrated that these residues are conserved between human and mouse PKM2 (Fig. 3D), supporting their functional relevance.

To evaluate the role of these sites in PKM2 oligomerization, PKM2 mutants in which K135, K166 and K270 were substituted with arginine (PKM2-3KR, mimicking constitutive desuccinylation) or glutamate (PKM2-3KE, mimicking constitutive succinylation) were generated. Cross-linking and non-reducing SDS-PAGE analysis showed that PKM2-3KR predominantly formed dimers with reduced tetramer levels, whereas PKM2-3KE favored the tetrameric state (Fig. 3E). These findings demonstrate that desuccinylation at K135, K166 and K270 promotes PKM2 dimerization. To determine whether the succinylation status of K135, K166 and K270 directly influences fibrotic phenotypes, WT PKM2, the 3KR mutant or the 3KE mutant in MRC-5 cells were overexpressed and fibrotic marker expression was assessed by western blotting. The 3KR mutant, which mimics constitutive desuccinylation and predominantly forms dimers, significantly increased α-SMA, vimentin and collagen I protein levels compared with WT PKM2. By contrast, the 3KE mutant, which mimics constitutive succinylation and favors the tetrameric state, did not elevate fibrotic marker expression (Fig. 3F). These findings establish a functional link between site-specific PKM2 desuccinylation and fibroblast activation.

Collectively, these results define a post-translational regulatory mechanism in which circCACNA1D promotes desuccinylation of PKM2 at conserved lysine residues, thereby

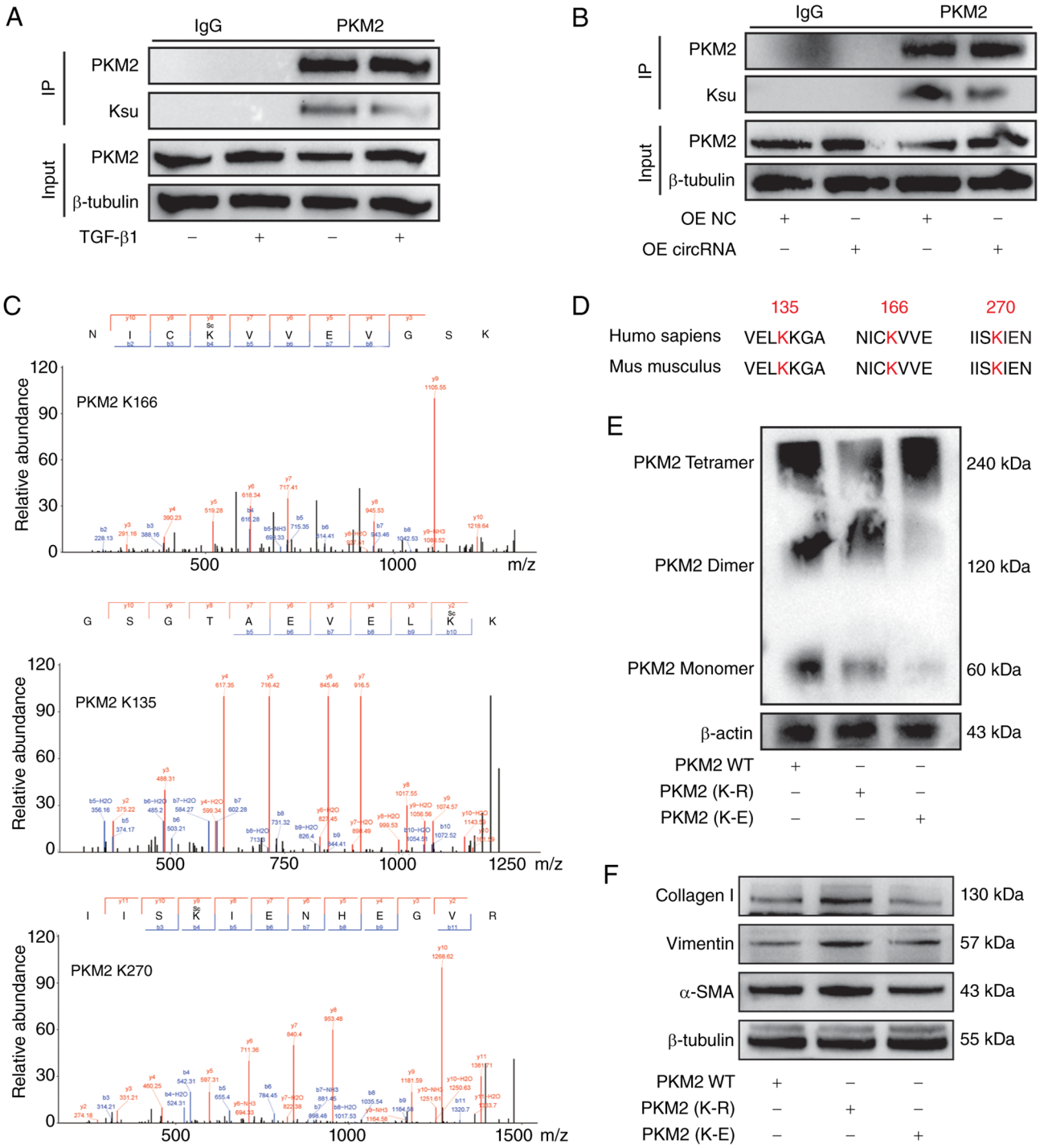

Figure 3. circCACNA1D promotes PKM2 desuccinylation at specific lysine residues to facilitate dimer formation. (A) Immunoprecipitation and western blot analysis of PKM2 succinylation (Ksu, succinyllysine) levels in MRC-5 cells treated with or without TGF-β1 (5 ng/ml; 48 h). Whole-cell lysate and IgG controls are shown. (B) Immunoprecipitation and western blot analysis of PKM2 succinylation (Ksu, succinyllysine) levels in MRC-5 cells following circCACNA1D overexpression. (C) Representative MS/MS spectra confirming succinyllysine modification at K135, K166 and K270 on PKM2 in lung tissues. (D) Sequence alignment of PKM2 protein sequences from humans and mice, highlighting conserved lysine residues (K135, K166 and K270) identified in panel C. (E) Chemical cross-linking followed by non-reducing SDS-PAGE and western blot analysis to assess the oligomeric state of WT PKM2 and its succinylation-mimetic mutants (3KR and 3KE). Positions of tetrameric (~240 kDa) and dimeric (~120 kDa) PKM2 are indicated. (F) Western blot analysis of α-SMA, vimentin and collagen I in MRC-5 cells transfected with PKM2 WT, PKM2 (K-R) or PKM2 (K-E). β-tubulin served as a loading control. WT, wild type; PKM2, pyruvate kinase M2; circRNA, circular RNA.

shifting PKM2 toward its pro-fibrotic, transcriptionally active dimeric conformation.

Pharmacological stabilization of PKM2 tetramers alleviates fibrotic phenotypes in vitro. The present study then investigated whether the pharmacological stabilization of PKM2 tetramers counteracts fibrotic activation. Treatment with the selective PKM2 tetramer stabilizer, TEPP-46, increased tetramer formation in a concentration-dependent manner in theTGF-β1-stimulated MRC-5 cells, as shown by cross-linking

and non-reducing SDS-PAGE (Fig. 4A). TEPP-46 significantly reduced the TGF-β1-induced upregulation of α-SMA, vimentin and collagen I at the protein level (Fig. 4B and C). Immunofluorescence staining further demonstrated that TEPP-46 attenuated TGF-β1-induced α-SMA-positive stress fiber formation (Fig. 4D). Functionally, TEPP-46 significantly suppressed TGF-β1-induced cell migration in scratch-wound healing assays (Fig. 4E and F). Real-time proliferation analysis using the IncuCyte S3 system revealed that TEPP-46 inhibited TGF-β1-driven fibroblast growth (Fig. 4G). Taken together, these data support the concept that the tetramer-dimer balance of PKM2 functions as a molecular switch in fibrotic activation and that pharmacological stabilization of PKM2 tetramers mitigates fibrotic responses *in vitro*.

TEPP-46 attenuates pulmonary fibrosis in a murine model of pulmonary fibrosis induced by BLM. To assess the therapeutic effect of stabilizing PKM2 tetramers *in vivo*, a murine model of pulmonary fibrosis induced by BLM was used. Beginning on day 3 following the administration of BLM, mice received TEPP-46 to promote PKM2 tetramer formation. TEPP-46 significantly improved BLM-induced lung dysfunction, as evidenced by increased FVC (Fig. 5A), decreased lung resistance (RL; Fig. 5B) and increased dynamic compliance (Fig. 5C).

Consistent with these functional improvements, TEPP-46 markedly reduced the expression of fibrotic markers in lung tissues. Western blot analysis of lung homogenates confirmed the reduced expression of α-SMA, vimentin and collagen I (Fig. 5D). Immunofluorescence analysis revealed the decreased expression of α-SMA in theTEPP-46-treated mice compared with vehicle-treated BLM controls (Fig. 5E). Histopathological evaluation further supported these findings. H&E staining revealed preserved alveolar structure and reduced inflammatory infiltration (Fig. 5F), while Masson's trichrome staining demonstrated reduced collagen deposition in TEPP-46-treated lungs (Fig. 5G). These *in vivo* results indicate that TEPP-46 alleviates pulmonary fibrosis and support PKM2 tetramer stabilization as a therapeutic strategy.

Profibrotic function of circCACNA1D is dependent on PKM2 nuclear dimerization. To define the functional association between circCACNA1D and PKM2 dimerization, gain- and loss-of-function rescue experiments were conducted. circCACNA1D OE enhanced fibroblast migration (Fig. 6A and B), promoted cell proliferation (Fig. 6C) and increased the expression of fibrotic markers (α-SMA, vimentin and collagen I; Fig. 6D). These pro-fibrotic effects were abolished by co-treatment with TEPP-46 (Fig. 6A-D). By contrast, circCACNA1D knockdown in TGF-β1-stimulated cells reduced migration (Fig. 6E and F), proliferation (Fig. 6G) and fibrotic marker expression (Fig. 6H). Reintroduction of nuclear-localized PKM2 (PKM2-NLS), which enforces a transcriptionally active nuclear dimeric state, restored the fibrotic phenotypes suppressed by circCACNA1D knockdown (Fig. 6E-H). The transfection efficiency of si-circCACNA1D and PKM2-NLS was verified using RT-qPCR and western blot analysis, respectively, prior to functional assays (as described in the Materials and methods section). These findings demonstrate that circCACNA1D promotes pulmonary fibrosis by facilitating PKM2 nuclear dimerization and this effect can be disrupted by stabilizing PKM2 tetramers.

The metabolic consequences of the circCACNA1D-PKM2 axis were then examined. As PKM2 dimerization alters glycolytic flux, pyruvate kinase activity, which primarily reflects tetrameric PKM2 function, was assessed. circCACNA1D OE significantly reduced pyruvate kinase activity, and this reduction was reversed by TEPP-46 (Fig. 6I). circCACNA1D OE also increased lactate secretion, a hallmark of enhanced aerobic glycolysis, whereas TEPP-46 suppressed this increase (Fig. 6J). These data indicate a metabolic shift from oxidative phosphorylation toward glycolysis following circCACNA1D-induced PKM2 dimerization.

To confirm that these metabolic effects depend on nuclear PKM2 dimers, rescue experiments under loss-of-function conditions were performed. circCACNA1D knockdown in TGF-β1-stimulated cells increased pyruvate kinase activity and decreased lactate production. Both effects were reversed by PKM2-NLS expression (Fig. 6K and L). Taken together, these findings demonstrate that the circCACNA1D/PKM2 axis drives glycolytic reprogramming. By promoting PKM2 dimerization and nuclear localization, circCACNA1D suppresses pyruvate kinase enzymatic activity and increases lactate production, thereby supporting the proliferative and biosynthetic demands of activated fibroblasts during fibrotic remodeling.

Nuclear PKM2 dimer drives a pro-fibrotic transcriptional program by directly activating target genes. In addition to its metabolic function, nuclear PKM2 functions as a transcriptional co-activator. Therefore, the present study then investigated whether circCACNA1D-induced nuclear PKM2 dimers regulate a pro-fibrotic transcriptional program. RNA sequencing of MRC-5 cells under four conditions (control, TGF-β1, TGF-β1 + vehicle and TGF-β1 + TEPP-46) identified 529 genes upregulated by TGF-β1 and 389 genes downregulated by TEPP-46, with 42 overlapping candidates (Fig. 7A and B). GO and KEGG analyses revealed enrichment in fibrosis-related processes, including cell-cycle progression, cell division and the p53 signaling pathway (Fig. 7C and D). A total of seven candidate genes associated with proliferation and fibrosis were selected for validation. The overexpression of PKM2-NLS induced the marked upregulation of KIF4A mRNA (>6-fold), identifying KIF4A as a primary transcriptional target of nuclear PKM2 (Fig. 7E). TGF-β1 increased KIF4A expression at both the mRNA and protein levels (Fig. 7F and G). PKM2-NLS OE also elevated KIF4A protein expression (Fig. 7H). Notably, TEPP-46 treatment suppressed TGF-β1-induced KIF4A expression at both the mRNA and protein levels (Fig. 7I and J). Functional assays revealed that KIF4A knockdown reduced the expression of fibrotic markers, including α-SMA, vimentin and collagen I (Fig. 7K). To further confirm KIF4A as a functional downstream effector of nuclear PKM2, KIF4A gain-of-function experiments were performed. The overexpression of KIF4A in MRC-5 cells increased the protein levels of fibrotic markers, including α-SMA, vimentin and collagen I (Fig. 7L). These data, together with the KIF4A knockdown results, establish that KIF4A is both necessary and sufficient to drive pro-fibrotic gene expression downstream of the circCACNA1D/PKM2 axis. ChIP-qPCR

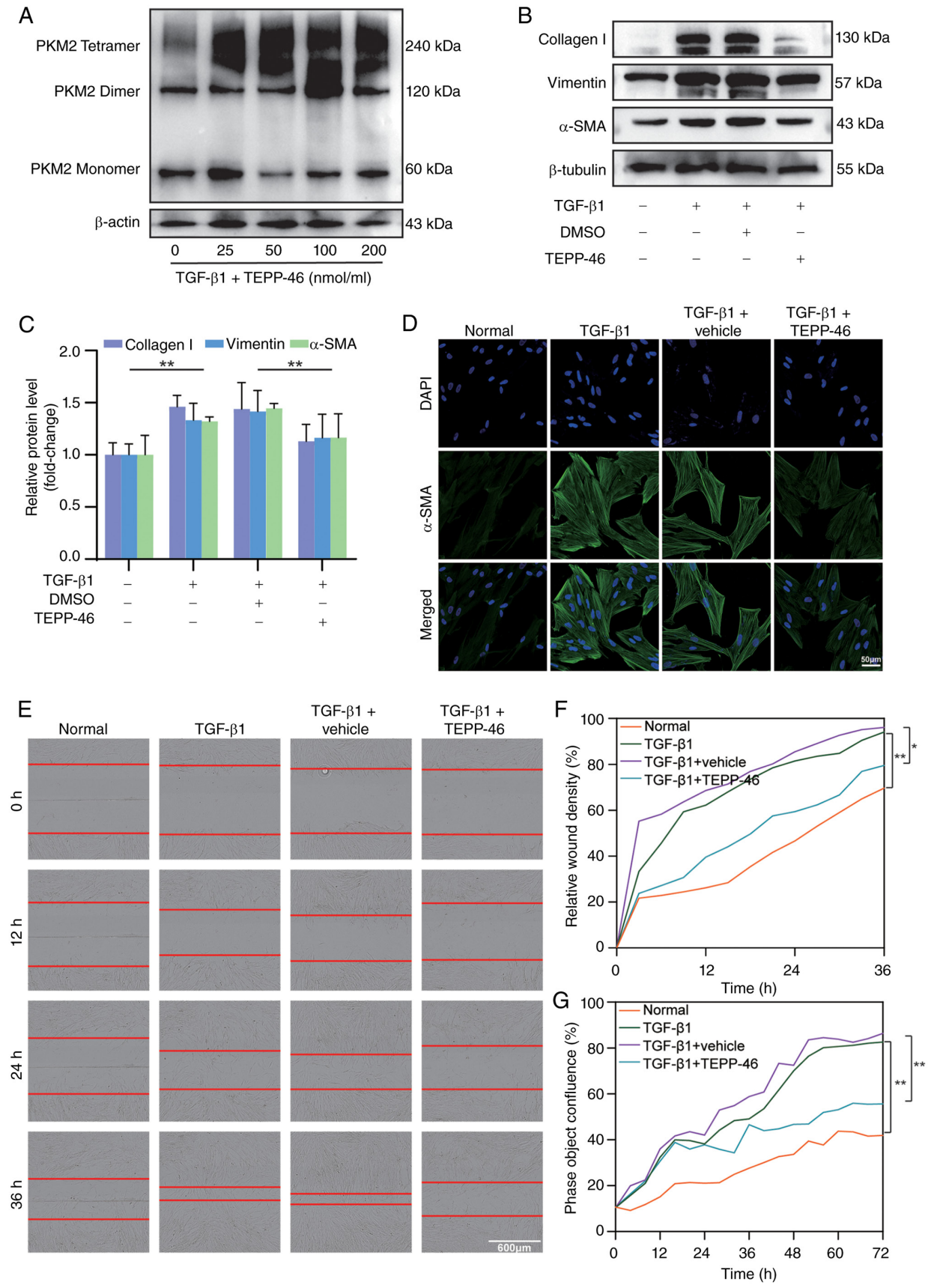

Figure 4. Pharmacological stabilization of PKM2 tetramers alleviates fibrotic phenotypes *in vitro*. (A) Non-reducing SDS-PAGE analysis of PKM2 oligomeric states in TGF-β1-stimulated MRC-5 cells treated with increasing concentrations of TEPP-46 (0, 25, 50, 100 and 200 nmol/ml). (B) Western blot analysis of fibrotic markers (α-SMA, vimentin and collagen I) in MRC-5 cells treated with TGF-β1 (5 ng/ml) in the presence or absence of TEPP-46 (50 nmol/ml). (C) Quantitative analysis of the results of western blot analysis. (D) Immunofluorescence staining of α-SMA (green) in MRC-5 cells under the indicated conditions. Nuclei were stained with DAPI (blue; scale bar, 50 μm). (E) Scratch-wound healing assay of MRC-5 cells treated with TGF-β1 and TEPP-46. (F) Quantitative analysis of wound closure. (G) Cell proliferation monitored by IncuCyte S3 live-cell analysis under the same conditions. *P<0.05, **P<0.01. PKM2, pyruvate kinase.

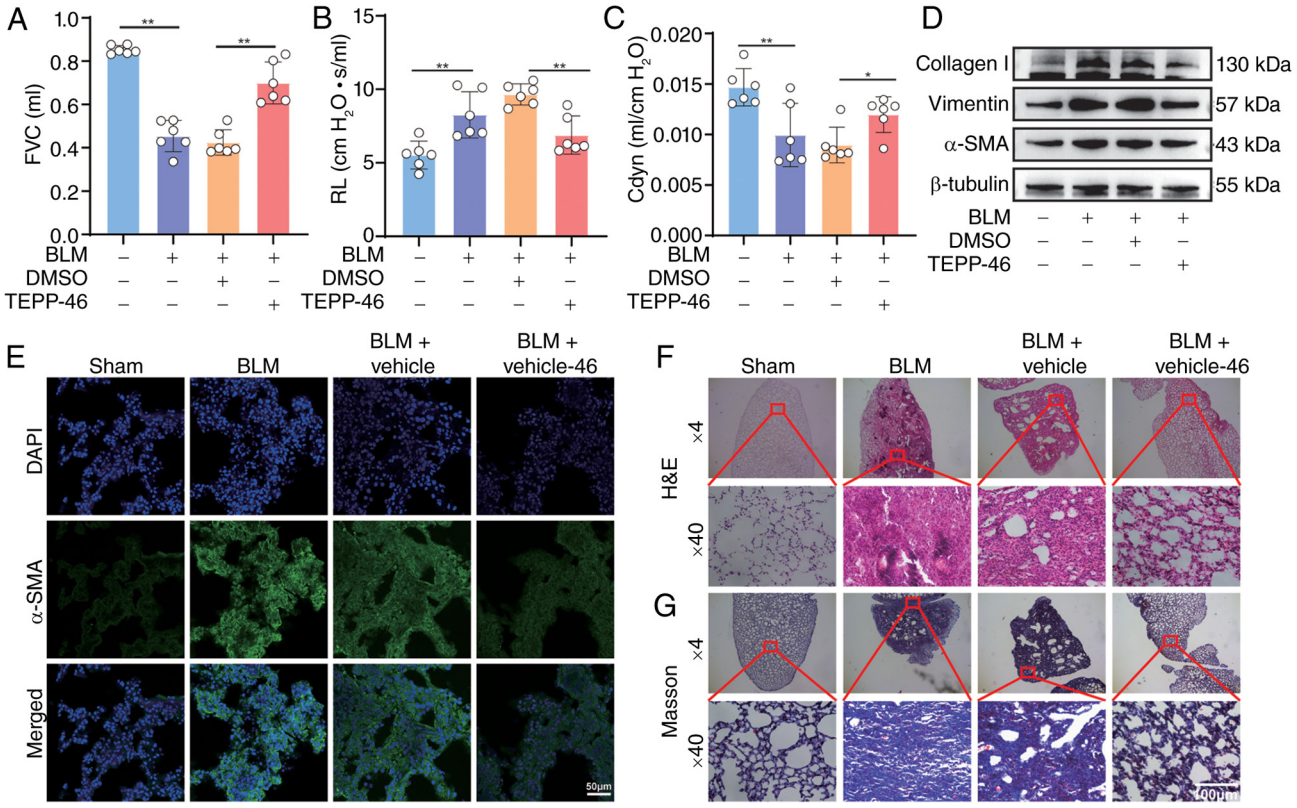

Figure 5. TEPP-46 attenuates BLM-induced pulmonary fibrosis in mice. (A) FVC measured on day 28 after BLM instillation in mice treated with saline (control), BLM alone, BLM + vehicle or BLM + TEPP-46. (B) RL assessed under the same treatment conditions as in (A). (C) Cdyn evaluated under the same treatment conditions as in (A). (D) Western blot analysis of α-SMA, vimentin and collagen I protein levels in lung tissue homogenates. β-tubulin served as a loading control. (E) Immunofluorescence staining of α-SMA in lung tissue sections (scale bar, 50 μm). (F) Histopathological assessment of lung sections by H&E staining. (G) Masson's trichrome staining of lung sections (scale bar, 100 μm). *P<0.05, **P<0.01. FVC, forced vital capacity; RL, lung resistance; Cdyn, dynamic compliance; BLM, bleomycin.

analysis demonstrated the direct enrichment of PKM2 at multiple regions of the KIF4A promoter under TGF-β1 stimulation (Fig. 7M), indicating increased DNA binding activity associated with the dimeric form. Of note, the KIF4A and PDZD11 genes are arranged in a head-to-head bidirectional configuration on the X chromosome, sharing an overlapping promoter region; therefore, the ChIP primers inevitably amplify both promoters. However, PDZD11 expression was not significantly altered by TGF-β1, TEPP-46, or PKM2-NLS overexpression (Fig. S2), confirming that the observed ChIP signals predominantly reflect PKM2 occupancy at the KIF4A locus. These findings identify KIF4A as a critical downstream effector of nuclear PKM2 dimers and establish a mechanistic link between PKM2-driven metabolic reprogramming and transcriptional activation in pulmonary fibrosis.

Discussion

The present study identified circCACNA1D as a novel regulator of PKM2 conformational switching in pulmonary fibrosis. The data support a model in which circCACNA1D directly binds PKM2, attenuates its succinylation at K135, K166 and K270, and shifts the enzyme toward the dimeric, transcriptionally competent state. Functionally, this conformational shift suppresses pyruvate kinase activity, increases lactate production, enhances fibroblast migration and proliferation, and promotes expression of fibrotic markers. At the transcriptional level, KIF4A was identified as a critical downstream effector of the circCACNA1D/PKM2 pathway. These findings are conceptually important as they extend circRNA biology beyond canonical miRNA-sponging mechanisms and demonstrate that a circRNA can directly reshape the biochemical state of a metabolic enzyme to coordinate metabolic and transcriptional remodeling in fibrosis (11,30).

The results of the present study also contribute to the increasing amount of literature implicating PKM2 in fibrotic diseases. Recent studies have demonstrated that PKM2 promotes pulmonary fibrosis by stabilizing TGF-β receptor I (16), drives fibrogenic metabolic rewiring in kidney injury (17,18), restrains or promotes fibrogenesis depending on its oligomeric state in hepatic stellate cells (19) and contributes to fibrosis-associated lactate accumulation in multiple organs (21,40,41). Together, these studies establish PKM2 as a major determinant of fibrotic remodeling. However, the majority of previous studies have focused on downstream consequences of PKM2 activation (42,43), while the upstream mechanisms governing its dimer-tetramer switching in pulmonary fibrosis remained unclear. The data from the present study indicate that circCACNA1D functions as an upstream regulator of PKM2 to couple post-transcriptional regulation to metabolic reprogramming and nuclear gene activation. This provides an explanation for the mechanisms by which fibroblasts sustain a stable profibrotic phenotype despite fluctuating extracellular signals.

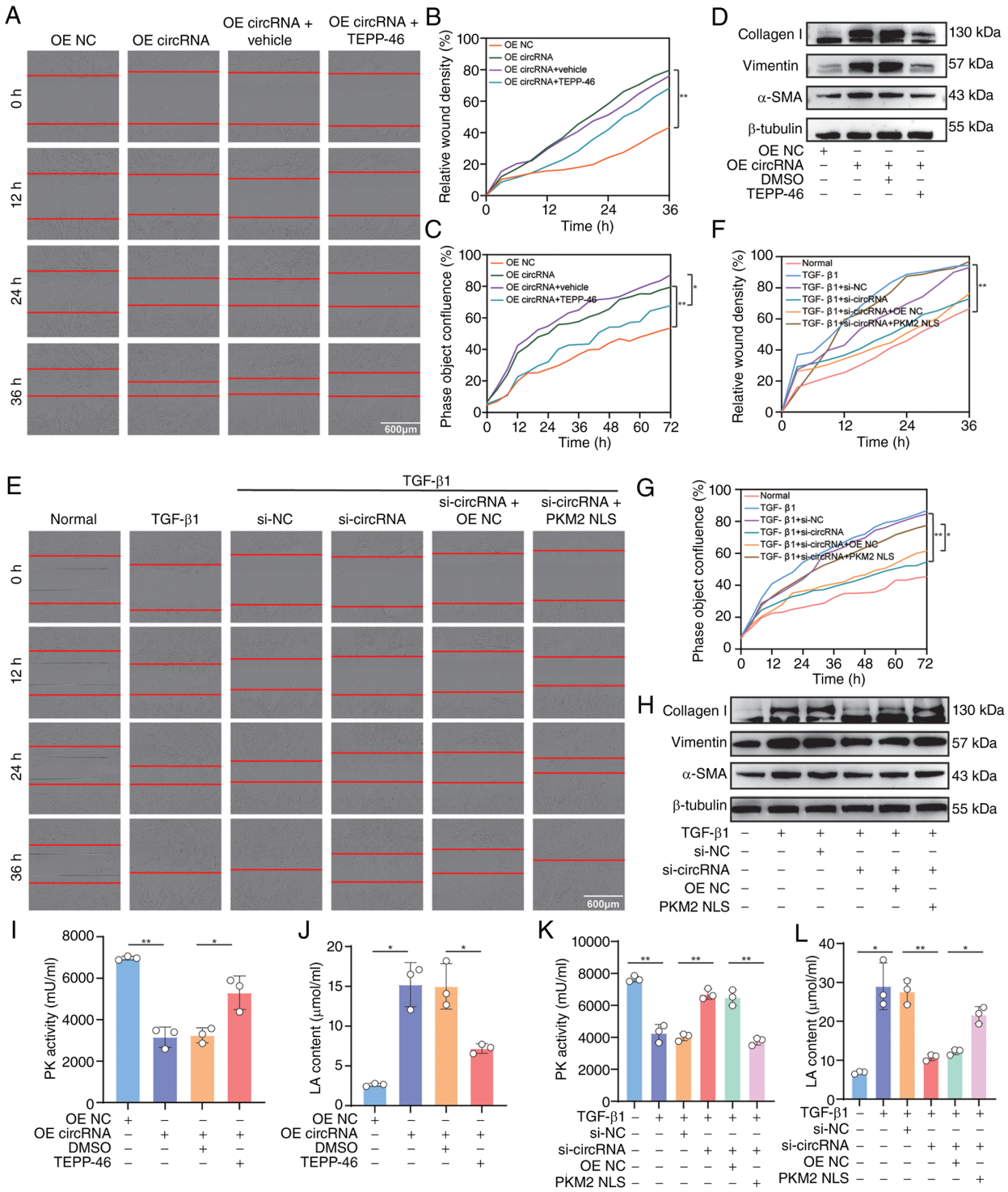

Figure 6. Pro-fibrotic function of circCACNA1D is dependent on PKM2 nuclear dimerization. (A) Scratch-wound healing assay illustrating the migration of MRC-5 cells overexpressing circCACNA1D with or without TEPP-46 (50 nmol/ml; scale bar, 600 μm). (B) Quantitative analysis of wound closure. (C) Cell proliferation of MRC-5 cells overexpressing circCACNA1D with or without TEPP-46 (50 nmol/ml), monitored by IncuCyte S3. (D) Western blot analysis of fibrotic markers (α-SMA, vimentin and collagen I) under the same conditions as in panel A. (E) Scratch-wound healing assay under TGF-β1 stimulation following circCACNA1D knockdown and rescue with PKM2-NLS. (F) Quantitative analysis of wound closure. (G) Cell proliferation under TGF-β1 stimulation following circCACNA1D knockdown and PKM2-NLS rescue. (H) Western blot analysis of fibrotic markers under the same experimental groups as those in panel E. (I) PK activity measured in MRC-5 cells overexpressing circCACNA1D or an empty vector control, with or without TEPP-46 (50 nmol/ml) for 48 h. (J) Lactate secretion in the cell culture supernatant under the same conditions as those in panel I. (K) PK activity assessed in MRC-5 cells treated with TGF-β1 (5 ng/ml; 48 h) with or without circCACNA1D knockdown,and rescued by PKM2-NLS overexpression. (L) Lactate secretion measured under the same treatment groups as in those in panel K. *P<0.05, **P<0.01. circRNA, circular RNA; PK, pyruvate kinase; PKM2-NLS, nuclear-localized PKM2.

A key question raised by the findings of the present study is why circCACNA1D is upregulated in fibrotic lungs. Although the present study did not directly elucidate the upstream regulatory mechanism, several non-mutually exclusive hypotheses merit consideration. First, chronic TGF-β/SMAD signaling may enhance the transcription of the CACNA1D host

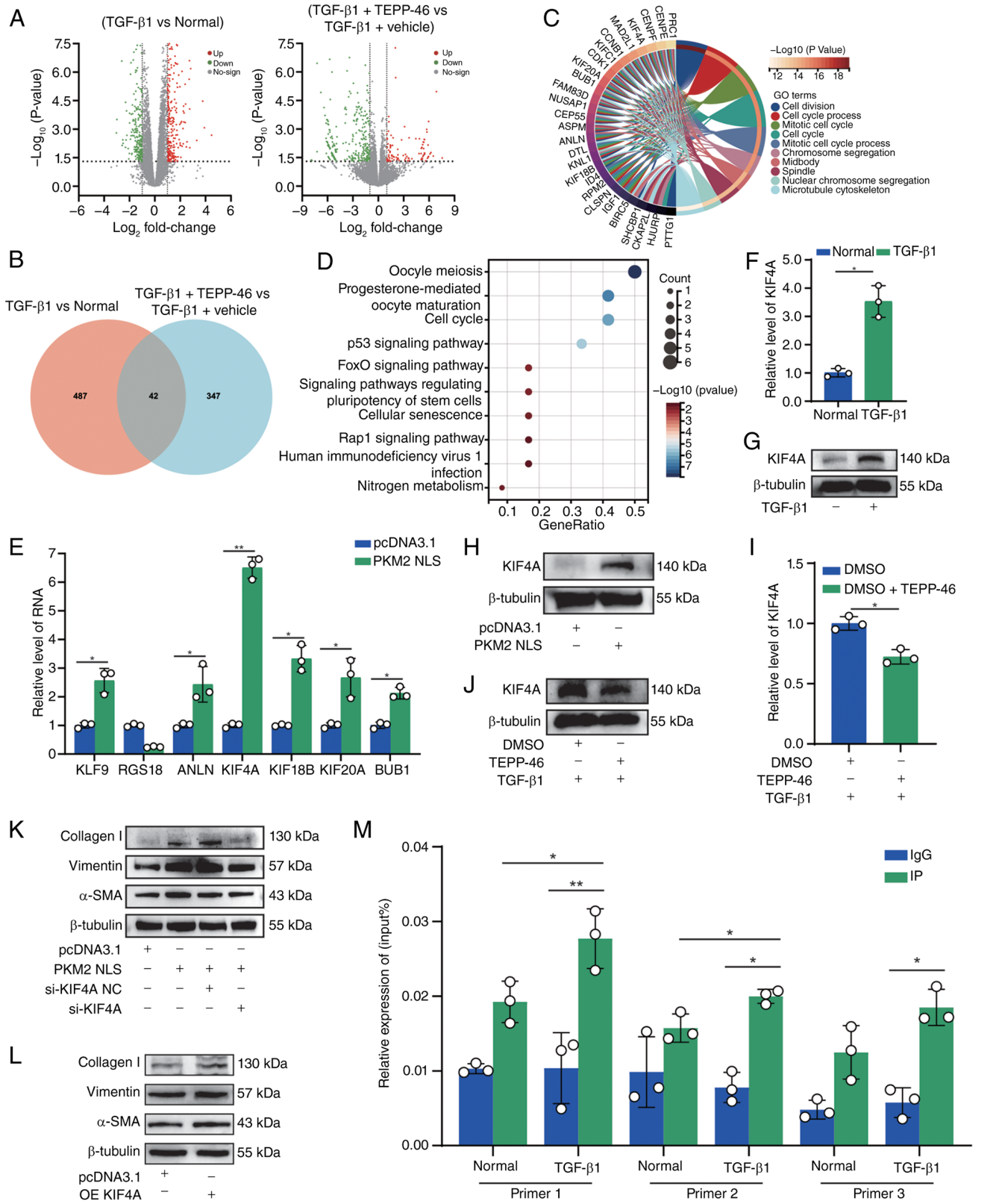

Figure 7. Nuclear PKM2 dimer drives a pro-fibrotic transcriptional program via direct activation of KIF4A. (A) Volcano plot of differentially expressed genes between control vs. TGF-β1 (left) and TGF-β1 + vehicle vs. TGF-β1 + TEPP-46 (right). (B) Venn diagram demonstrating overlap between TGF-β1-upregulated (529) and TEPP-46-downregulated (389) genes, yielding 42 candidates. (C) GO enrichment analysis of the 42 overlapping genes. (D) KEGG pathway enrichment analysis of the same gene set. (E) qPCR validation of candidate gene expression in cells overexpressing PKM2-NLS. (F) qPCR analysis of KIF4A mRNA levels under the indicated treatments. (G) Western blot analysis of KIF4A protein levels under the same conditions as those in panel F. (H) Western blot analysis of KIF4A protein levels under PKM2-NLS overexpression. (I) qPCR analysis of KIF4A mRNA levels with TEPP-46 treatment. (J) Western blot analysis of KIF4A protein levels under the same conditions as those in panel I. (K) Western blot analysis of fibrotic markers (α-SMA, vimentin and collagen I) in MRC-5 cells overexpressing PKM2-NLS with or without concurrent KIF4A knockdown (siKIF4A). (L) Western blot analysis of fibrotic markers (α-SMA, vimentin and collagen I) in MRC-5 cells overexpressing KIF4A or an empty vector control. β-tubulin served as a loading control. (M) ChIP-qPCR showing PKM2 enrichment at the KIF4A promoter region in TGF-β1-stimulated MRC-5 cells. *P<0.05, **P<0.01. PKM2, pyruvate kinase; KIF4A, kinesin family member 4A; GO, Gene Ontology; KEGG, Kyoto Encyclopedia of Genes and Genomes; PKM2-NLS, nuclear-localized PKM2; ChIP-qPCR, chromatin immunoprecipitation quantitative PCR.

locus or alter local chromatin architecture, thereby favoring circular RNA production (44). Second, fibrosis-associated RNA-binding proteins that regulate back-splicing may increase circCACNA1D biogenesis under stress conditions (45). Third, epitranscriptomic regulation may contribute, as m^6A modification has been implicated in circRNA processing, export and stability (46). These hypotheses are not mutually exclusive, and determining which mechanism predominates will be key for understanding how the circCACNA1D-PKM2 axis is engaged during disease initiation and progression.

A central mechanistic finding of the present study is that circCACNA1D promotes PKM2 desuccinylation. The mutational data support the functional importance of K135, K166 and K270 in controlling PKM2 oligomerization, as the desuccinylation-mimetic 3KR mutant favored dimer formation and enhanced fibrotic marker expression, whereas the succinylation-mimetic 3KE mutant favored tetramer formation and exhibited diminished profibrotic activity. These observations position succinylation among other PTMs as a key determinant of PKM2 structural and functional plasticity (23,47-49). Notably, the present study demonstrated the consequence of circCACNA1D binding, but did not fully define the molecular mechanism by which desuccinylation occurs. One plausible model is a scaffold mechanism, in which circCACNA1D facilitates the association of PKM2 with a desuccinylase, such as SIRT5, thereby promoting targeted removal of succinyl groups (35,50). An alternative, non-mutually exclusive model is steric regulation, whereby circCACNA1D binding alters the local conformation of PKM2 or limits the accessibility of these lysine residues to succinylation machinery or succinyl-CoA (51). At present, the data from the present study support a circCACNA1D-dependent desuccinylation process; however, additional biochemical studies will be required to distinguish whether the recruitment of a desuccinylase, the steric exclusion of succinylation or a combination of both underlies this phenomenon.

The results of the present study also underscore the importance of contextualizing PKM2 succinylation within a broader PTM network, rather than as an isolated event. PKM2 is extensively regulated via phosphorylation, acetylation, oxidation, lysine acylation and protein-partner interactions, all of which can influence its enzymatic activity, subcellular localization or non-metabolic signaling functions (9,11). Recent studies have shown that S-nitrosylation can promote PKM2 dimerization in cardiac fibrosis (47), succinate-driven succinylation can accelerate age-associated fibrotic remodeling (23) and diverse binding partners can redirect PKM2 toward noncanonical transcriptional outputs (48,49). Consequently, it is plausible that distinct PTMs and interacting proteins cooperate or compete to determine whether PKM2 adopts a catalytically active tetrameric state or a signaling-competent dimeric state in fibroblasts. Systematic mapping of PTM crosstalk on PKM2 in fibrotic cells is essential to elucidate the mechanisms by which metabolic reprogramming becomes stabilized during chronic tissue injury.

A notable contribution of the present study is the expansion of the emerging field of circRNA-mediated metabolic regulation. Several circRNAs have already been implicated in pulmonary fibrosis, but most act indirectly through ceRNA circuits or upstream signaling pathways. For example, circHIPK3 promotes pulmonary fibrosis by facilitating glycolysis through a miR-30a-3p/FOXK2-dependent mechanism (3), while previous research has demonstrated that circ0066187/circCACNA1D can also promote pulmonary fibrogenesis through STAT3-associated metabolic signaling (33). By contrast, the present study established a direct circRNA-protein regulatory mechanism, in which circCACNA1D binds PKM2 and modulates its post-translational and oligomeric state. This mechanism is distinct from recently described circRNA-PKM2 signaling in other disease contexts. For instance, circABCC4 in pancreatic cancer-associated fibroblasts drives glycolytic reprogramming and chemoresistance by promoting PKM2 nuclear translocation through KPNA2 recruitment (52), whereas other non-coding RNAs or protein partners influence PKM2 activity through different structural or catalytic mechanisms (49,53). Thus, circCACNA1D regulates PKM2 through a mechanism governed by succinylation-dependent dimer-tetramer switching, rather than solely on transcript abundance or trafficking adaptors. This mechanistic distinction underscores the novelty of the present study.

At the transcriptional level, the present study identified KIF4A as a pivotal downstream effector of the circCACNA1D/PKM2 axis. Nuclear PKM2 is increasingly recognized as a signaling hub that couples metabolic state to gene regulation (11,54), and the RNA-seq, gain-of-function, loss-of-function and ChIP-qPCR data of the present study collectively substantiate KIF4A as a functionally relevant target in fibrotic fibroblasts. However, KIF4A is unlikely to be the sole effector of nuclear PKM2 in this setting. Rather, it likely constitutes part of a broader transcriptional program through which dimeric PKM2 drives proliferation, matrix production and fibroblast persistence. Genome-wide chromatin occupancy and target-gene analyses are required to define this network more comprehensively.

From a translational perspective, the findings of the present study underscore the therapeutic potential of PKM2 conformational control. TEPP-46, a selective PKM2 activator that stabilizes the tetrameric state, abrogated the profibrotic effects of circCACNA1D *in vitro* and attenuated BLM-induced pulmonary fibrosis *in vivo* (18). These observations suggest that the dimeric and nuclear forms of PKM2 are not simply a byproduct of metabolic stress, but an active driver of fibrotic pathology. More broadly, they suggest that promoting tetrameric PKM2 may represent a viable antifibrotic strategy, particularly in disease contexts characterized by persistent glycolytic rewiring and pathological nuclear PKM2 signaling.

The present study has several limitations. First, although the present study established PKM2 desuccinylation as a key regulatory event downstream of circCACNA1D, the specific desuccinylase responsible has not yet been identified nor have any additional PKM2 PTMs which are involved in this regulatory mechanism. Second, the upstream mechanisms leading to circCACNA1D upregulation in fibrosis remain to be elucidated. Third, although KIF4A was validated herein as a critical downstream effector, nuclear PKM2 likely regulates additional genes relevant to fibroblast activation. Finally, investigating the applicability of this pathway to other fibrotic organs and validation in larger human cohorts will be important for defining its broader translational importance.

In conclusion, a pathogenic circCACNA1D-PKM2 signaling axis in pulmonary fibrosis was identified in the present study. By promoting PKM2 desuccinylation and shifting the dimer-tetramer equilibrium toward the dimeric state, circCACNA1D couples glycolytic reprogramming with nuclear transcriptional activation, thereby driving fibroblast activation. These findings deepen the understanding of the mechanisms by which non-coding RNAs directly regulate metabolic enzymes in fibrotic disease and highlight PKM2 conformational control as a potentially druggable vulnerability in pulmonary fibrosis.

Acknowledgements

Not applicable.

Funding

The present study was supported by the Special Funding for the 'Case-by-Case Introduction of Top Talent (Teams)' Program in Yantai, China. The present study was also funded by the National Natural Science Foundation of China (grant nos. 82500104, 82400117, 82370079, 82370094, 82170085, 81970064 and 81870001).

Availability of data and materials

The data generated in the present study may be requested from the corresponding author. The mass spectrometry proteomics data have been submitted to the ProteomeXchange Consortium through the PRIDE partner repository with the dataset identifier PXD075455, and are accessible at https://www.ebi.ac.uk/pride/archive/projects/PXD075455. The raw sequencing data generated in this study are openly available in the NCBI SRA database accessible with the following link: https://www.ncbi.nlm.nih.gov/sra/PRJNA1475466.

Authors' contributions

SZ, XS and JZ designed the study. YW, XL and JZ performed the experiments, analyzed the data, and wrote the manuscript. MW and NZ contributed to the conception and design of the study. MJ assisted with the animal experiments and data collection. BL participated in the study design and interpretation of data. CL participated in the data analysis and critical review of the manuscript. SZ and XS prepared the figures and revised the manuscript. SZ and XS confirm the authenticity of all the raw data. All authors have read and approved the final manuscript.

Ethics approval and consent to participate

All animal procedures were approved by the Animal Ethics Committee of Shandong Medical and Pharmaceutical University (approval no. 2021-355).

Patient consent for publication

Not applicable.

Competing interests

The authors declare that they have no competing interests.

References

1. Li J, Li P, Zhang G, Qin P, Zhang D and Zhao W: CircRNA TADA2A relieves idiopathic pulmonary fibrosis by inhibiting proliferation and activation of fibroblasts. Cell Death Dis 11: 553, 2020.
2. Hong SH, Yun B, Cho S, Hong OY, Lee SH, Kim WH and Hong JY: Loss of ATF3 exacerbates pulmonary fibrosis via enhanced neutrophil recruitment and profibrotic macrophage polarization. Clin Sci (Lond) 140: 179-199, 2026.
3. Xu Q, Cheng D, Li G, Liu Y, Li P, Sun W, Ma D and Ni C: CircHIPK3 regulates pulmonary fibrosis by facilitating glycolysis in miR-30a-3p/FOXK2-dependent manner. Int J Biol Sci 17: 2294-2307, 2021.
4. Li J, Zhai X, Sun X, Cao S, Yuan Q and Wang J: Metabolic reprogramming of pulmonary fibrosis. Front Pharmacol 13: 1031890, 2022.
5. Richeldi L, Baldi F, Pasciuto G, Macagno F and Panico L: Current and future idiopathic pulmonary fibrosis therapy. Am J Med Sci 357: 370-373, 2019.
6. Koudstaal T and Wijsenbeek MS: Idiopathic pulmonary fibrosis. Presse Med 52: 104166, 2023.
7. Bueno M, Calyeca J, Rojas M and Mora AL: Mitochondria dysfunction and metabolic reprogramming as drivers of idiopathic pulmonary fibrosis. Redox Biol 33: 101509, 2020.
8. Li Z, Sun C and Qin Z: Metabolic reprogramming of cancer-associated fibroblasts and its effect on cancer cell reprogramming. Theranostics 11: 8322-8336, 2021.
9. Lv S, Cao M, Luo J, Fu K and Yuan W: Search progress of pyruvate kinase M2 (PKM2) in organ fibrosis. Mol Biol Rep 51: 389, 2024.
10. Vander Heiden MG, Cantley LC and Thompson CB: Understanding the Warburg effect: The metabolic requirements of cell proliferation. Science 324: 1029-1033, 2009.
11. Chen TJ, Wu CH, Hung MC, Wang WC and Kung HJ: Nuclear PKM2: A signal receiver, a gene programmer, and a metabolic modulator. J Biomed Sci 32: 75, 2025.
12. Israelsen WJ and Vander Heiden MG: Pyruvate kinase: Function, regulation and role in cancer. Semin Cell Dev Biol 43: 43-51, 2015.
13. Dayton TL, Jacks T and Vander Heiden MG: PKM2, cancer metabolism, and the road ahead. EMBO Rep 17: 1721-1730, 2016.
14. Christofk HR, Vander Heiden MG, Harris MH, Ramanathan A, Gerszten RE, Wei R, Fleming MD, Schreiber SL and Cantley LC: The M2 splice isoform of pyruvate kinase is important for cancer metabolism and tumour growth. Nature 452: 230-233, 2008.
15. Zhang Z, Zheng L, Chen Y, Chen Y, Hou J, Xiao C, Zhu X, Zhao SM and Xiong JW: AARS2 ameliorates myocardial ischemia via fine-tuning PKM2-mediated metabolism. Elife 13: RP99670, 2025.
16. Gao S, Li X, Jiang Q, Liang Q, Zhang F, Li S, Zhang R, Luan J, Zhu J, Gu X, *et al*: PKM2 promotes pulmonary fibrosis by stabilizing TGF-β1 receptor I and enhancing TGF-β1 signaling. Sci Adv 8: eabo0987, 2022.
17. Chen Y, Bai X, Chen J, Huang M, Hong Q, Ouyang Q, Sun X, Zhang Y, Liu J, Wang X, *et al*: Pyruvate kinase M2 regulates kidney fibrosis through pericyte glycolysis during the progression from acute kidney injury to chronic kidney disease. Cell Prolif 57: e13548, 2024.
18. Liu H, Takagaki Y, Kumagai A, Kanasaki K and Koya D: The PKM2 activator TEPP-46 suppresses kidney fibrosis via inhibition of the EMT program and aberrant glycolysis associated with suppression of HIF-1α accumulation. J Diabetes Investig 12: 697-709, 2021.
19. Zheng D, Jiang Y, Qu C, Yuan H, Hu K, He L, Chen P, Li J, Tu M, Lin L, *et al*: Pyruvate kinase M2 tetramerization protects against hepatic stellate cell activation and liver fibrosis. Am J Pathol 190: 2267-2281, 2020.
20. Rao J, Wang H, Ni M, Wang Z, Wang Z, Wei S, Liu M, Wang P, Qiu J, Zhang L, *et al*: FSTL1 promotes liver fibrosis by reprogramming macrophage function through modulating the intracellular function of PKM2. Gut 71: 2539-2550, 2022.

21. Xu Y, Ma X, Ni W, Zheng L, Lin Z, Lai Y, Yang N, Dai Z, Yao T, Chen Z, *et al*: PKM2-driven lactate overproduction triggers endothelial-to-mesenchymal transition in ischemic flap via mediating TWIST1 lactylation. Adv Sci (Weinh) 11: e2406184, 2024.
22. Zhang Z, Tan M, Xie Z, Dai L, Chen Y and Zhao Y: Identification of lysine succinylation as a new post-translational modification. Nat Chem Biol 7: 58-63, 2011.
23. Wang Z, Zhang Z, Ping Z, Yang S, Li Y, Jiang T, Zheng X, Zhang Q, Liu Z, Zhang X, *et al*: Succinate-driven PKM2 succinylation and dimerization accelerates age-associated cardiac fibrosis. Commun Biol 9: 633, 2025.
24. Wang F, Wang K, Xu W, Zhao S, Ye D, Wang Y, Xu Y, Zhou L, Chu Y, Zhang C, *et al*: SIRT5 desuccinylates and activates pyruvate kinase M2 to block macrophage IL-1β production and to prevent DSS-induced colitis in mice. Cell Rep 19: 2331-2344, 2017.
25. Du J, Zhou Y, Su X, Yu JJ, Khan S, Jiang H, Kim J, Woo J, Kim JH, Choi BH, *et al*: Sirt5 is a NAD-dependent protein lysine demalonylase and desuccinylase. Science 334: 806-809, 2011.
26. Zhang L, Lv T, Hou P, Jin Y and Jia F: Sirt5-mediated polarization and metabolic reprogramming of macrophage sustain brain function following ischemic stroke. Brain Res 1857: 149613, 2025.
27. Zhao Q, Jing Y, Jiang X, Zhang X, Liu F, Huang H, Zhang Z, Wang H, Sun S, Ma S, *et al*: SIRT5 safeguards against primate skeletal muscle ageing via desuccinylation of TBK1. Nat Metab 7: 556-573, 2025.
28. Song Z, Zhou M, Lin J, You J and Huang C: Translatable circular RNAs: Mechanism, function and clinical application. Int J Biol Macromol 335: 149185, 2026.
29. Huang A, Zheng H, Wu Z, Chen M and Huang Y: Circular RNA-protein interactions: Functions, mechanisms, and identification. Theranostics 10: 3503-3517, 2020.
30. Dong J, Zeng Z, Huang Y, Chen C, Cheng Z and Zhu Q: Challenges and opportunities for circRNA identification and delivery. Crit Rev Biochem Mol Biol 58: 19-35, 2023.
31. Chen LL: The expanding regulatory mechanisms and cellular functions of circular RNAs. Nat Rev Mol Cell Biol 21: 475-490, 2020.
32. Rochow H, Franz A, Jung M, Weickmann S, Ralla B, Kilic E, Stephan C, Fendler A and Jung K: Instability of circular RNAs in clinical tissue samples impairs their reliable expression analysis using RT-qPCR: From the myth of their advantage as biomarkers to reality. Theranostics 10: 9268-9279, 2020.
33. Liu B, Liu W, Li H, Zhai N, Lv C, Song X and Yang S: circ0066187 promotes pulmonary fibrogenesis through targeting STAT3-mediated metabolism signal pathway. Cell Mol Life Sci 82: 79, 2025.
34. You Q, Yu J, Pan R, Feng J, Guo H and Liu B: Decoding the regulatory roles of circular RNAs in cardiac fibrosis. Noncoding RNA Res 11: 115-130, 2024.
35. Zhou WY, Cai ZR, Liu J, Wang DS, Ju HQ and Xu RH: Circular RNA: Metabolism, functions and interactions with proteins. Mol Cancer 19: 172, 2020.
36. Shen Y, Zhang N, Chai J, Wang T, Ma C, Han L and Yang M: CircPDIA4 induces gastric cancer progression by promoting ERK1/2 activation and enhancing biogenesis of oncogenic circRNAs. Cancer Res 83: 538-552, 2023.
37. Livak KJ and Schmittgen TD: Analysis of relative gene expression data using real-time quantitative PCR and the 2(-Delta Delta C(T)) method. Methods 25: 402-408, 2001.
38. Wang Y, Zhao Y, Cao G, Jiang M, Yuan X, Li H, Song X, Zhang J, Lv C and Zhang S: STAT3 facilitates super enhancer formation to promote fibroblast-to-myofibroblast differentiation by the analysis of ATAC-Seq, RNA-Seq and ChIP-Seq. J Cell Mol Med 29: e70639, 2025.
39. Zhang J, Wang H, Chen H, Li H, Xu P, Liu B, Zhang Q, Lv C and Song X: ATF3-activated accelerating effect of LINC00941/lncIAPF on fibroblast-to-myofibroblast differentiation by blocking autophagy depending on ELAVL1/HuR in pulmonary fibrosis. Autophagy 18: 2636-2655, 2022.
40. Xiang T, Wang X, Huang S, Zhou K, Fei S, Zhou B, Yue K, Li Q, Xue S, Dai Y, *et al*: Inhibition of PKM2 by shikonin impedes TGF-β1 expression by repressing histone lactylation to alleviate renal fibrosis. Phytomedicine 136: 156324, 2025.
41. Liu JY, Liao W, Chen ZY, Liu T, Wang R, Gong JP, Xu XS and Wu H: PKM2 drives lactate-mediated fibrosis in liver transplantation. Transplantation 109: e631-e646, 2025.
42. Wang Y, Hu R, Zhang X, Cai G, Ding Q and Che P: PKM2 mediates the glycolytic response to matrix stiffness in lung fibroblasts. Front Cell Dev Biol 14: 1771078, 2026.
43. Feng J, Huang X, Peng Y, Yang W, Yang X, Tang R, Xu Q, Gao Y, He Z, Xing S and Mei S: Pyruvate kinase M2 modulates mitochondrial dynamics and EMT in alveolar epithelial cells during sepsis-associated pulmonary fibrosis. J Transl Med 23: 205, 2025.
44. Gélabert C, Papoutsoglou P, Golán I, Ahlström E, Ameur A, Heldin CH, Caja L and Moustakas A: The long non-coding RNA LINC00707 interacts with Smad proteins to regulate TGFβ signaling and cancer cell invasion. Cell Commun Signal 21: 271, 2023.
45. Chiusa M, Lee YA, Zhang MZ, Harris RC, Sherrill T, Lindner V, Brooks CR, Yu G, Fogo AB, Flynn CR, *et al*: Cytoplasmic retention of the DNA/RNA-binding protein FUS ameliorates organ fibrosis in mice. J Clin Invest 134: e175158, 2024.
46. Di Timoteo G, Dattilo D, Centrón-Broco A, Colantoni A, Guarnacci M, Rossi F, Incarnato D, Oliviero S, Fatica A, Morlando M and Bozzoni I: Modulation of circRNA metabolism by m^6A modification. Cell Rep 31: 107641, 2020.
47. Luo S, Ye D, Zhang Y, Wang Y, Zhou M, Lv M, Wang X, Zhong K, Zhang Y, Hu L, *et al*: S-Nitrosylation of pyruvate kinase isoform 2 drives cardiac fibrosis by promoting mitochondrial fission. Circulation 153: 338-357, 2026.
48. Wu Y, Tang L, Huang H, Yu Q, Hu B, Wang G, Ge F, Yin T, Li S and Yu X: Phosphoglycerate dehydrogenase activates PKM2 to phosphorylate histone H3T11 and attenuate cellular senescence. Nat Commun 14: 1323, 2023.
49. Yu JT, Xie SS, Shen XY, Li Z, Hu XW, Zhang Y, Dong ZH, Wang JN, Li XY, Dong YH, *et al*: Renal tubular epithelial IGFBP7 interacts with PKM2 to drive renal lipid accumulation and fibrosis. Mol Ther 33: 3757-3777, 2025.
50. Wang J, Gao J, Ding L, Yang X, Zheng D, Zeng Y, Zhu J, Lei W, Chen C, Liu Z and Huang JA: Circular RNA-cacna1d plays a critical role in sepsis-induced lung injury by sponging microRNA-185-5p. Am J Respir Cell Mol Biol 72: 181-194, 2025.
51. Sandoval JE, Carullo NVN, Salisbury AJ, Day JJ and Reich NO: Mechanism of non-coding RNA regulation of DNMT3A. Epigenetics Chromatin 18: 15, 2025.
52. He R, Hu C, Yuan Y, Li T, Tian Q, Huang T, Lin Q, Zheng S, Chen C, Fu Z and Chen R: Glycolysis reprogramming in CAFs promotes oxaliplatin resistance in pancreatic cancer through circABCC4 mediated PKM2 nuclear translocation. Cell Death Dis 16: 126, 2025.
53. Fei M, Li X, Liang S, Zhou S, Wu H, Sun L, Liu Y, Hu Q, Liu L and Wang J: LncRNA PWRN1 inhibits the progression of hepatocellular carcinoma by activating PKM2 activity. Cancer Lett 584: 216620, 2024.
54. Yang W, Xia Y, Ji H, Zheng Y, Liang J, Huang W, Gao X, Aldape K and Lu Z: Nuclear PKM2 regulates β-catenin transactivation upon EGFR activation. Nature 480: 118-122, 2011.